Communication

Tamm Plasmons in TiO$_2$ Nanotube Photonic Crystals

Maxim V. Pyatnov [1,2,*] (ID)**, Rashid G. Bikbaev [1,2]** (ID)**, Ivan V. Timofeev [1,2]** (ID)**, Ilya I. Ryzhkov [2,3]** (ID)**,
Stepan Ya. Vetrov [1,2]** (ID) **and Vasily F. Shabanov [1]**

[1] Kirensky Institute of Physics, Krasnoyarsk Scientific Center, Siberian Branch, Russian Academy of Sciences, 660036 Krasnoyarsk , Russia
[2] Siberian Federal University, 660041 Krasnoyarsk, Russia
[3] Institute of Computational Modelling, Krasnoyarsk Scientific Center, Siberian Branch, Russian Academy of Sciences, 660036 Krasnoyarsk, Russia
[*] Correspondence: makspyatnov@yandex.ru

Abstract: The anodic TiO$_2$ photonic crystals evoke great interest for application as photocatalytic media due to high absorption of light resuling from their specific structure. In this work, the optical properties of the photonic crystal based on a bamboo-type TiO$_2$ nanotube with a metallic coating are analyzed theoretically by the finite-difference time-domain method. The occurrence of Tamm plasmons that appears as a peak in the absorption spectrum is predicted. A Tamm plasmon polariton is a localized state of light excited at the boundary of two highly reflective media, a metal and a Bragg reflector. The integral absorption of the gold-, titanium-, and titanium nitride-coated photonic crystals in the wavelength range of 450–600 nm is calculated. It is established that the titanium nitride-coated structure exhibits the maximum integral absorption.

Keywords: photonic crystals; titanium dioxide; absorbers; anodization

1. Introduction

The enhancement of light harvesting efficiency is a challenging task of modern nanophotonics, which should be resolved to improve the performance of various optoelectronic devices used in photovoltaics and photocatalysis.

A Tamm plasmon polariton (TPP) predicted theoretically in 2005 [1–3] and implemented in 2008 [4,5] is a localized state of light at the interface between a metallic layer and a photonic crystal (PC). The fundamental difference between a TPP and a resonator mode is that, in a TPP, the electromagnetic field is localized with the maximum at the interface between media and decays exponentially on both sides of it. Spectrally, a TPP manifests itself as a band in the reflectance, transmittance, and absorptance spectra of a sample. A TPP has certain advantages over a surface plasmon polariton [6,7], specifically:

- The TPP dispersion lies inside the light cone [1], which makes it possible to excite the localized state without prisms and gratings.
- A TPP can be formed in both the TE and TM polarizations.
- A TPP allows the resonance frequency control through a change in the parameters of a system [8].

The enduring interest in this phenomenon is due to a wide range of TPP applications, which include sensors [9–14], filters [15,16], lasers [17,18], absorbers [19–21], and solar cells [22,23].

A TPP can manifest itself not only as a narrow high-Q resonance, but also as a broad band in the reflectance, transmittance, and absorptance spectra. In this case, the resonance width is comparable with the band gap of a PC. Such a low-Q resonance is excited at the interface with a strongly absorbing metal, e.g., Al, Cr, or Ti [24].

Recently, we have proposed a design of a cell electrode consisting of a chirped PC and a thin titanium nitride layer separated by a semiconductor layer for light-induced water

splitting [25]. A broadband TPP excited in the structure causes the occurrence of a broad absorption band in the spectrum of the structure, which can be used in photocatalysis.

Photonic crystals are obtained conventionally by self-assembly (opal-like and liquid-crystal PCs), physical and chemical layer-by-layer vapor deposition (for 1D PCs in the form of Bragg mirrors), etching, photolithography, holographic methods, etc. [26]. Anodization of metal foil occupies a worthy place among the PC synthesis techniques due to its simplicity and low cost. The method is based on the transmission of an electric current between an anode and a cathode immersed in an electrolyte. A nanoporous oxide grows on the anode surface. The periodic voltage or current variation ensures the formation of periodic structures with a period commensurable with the optical radiation wavelength. The materials most frequently used in the fabrication of anodic PCs are silicon [27], aluminum [28], and titanium [29]. Titanium exhibits the excellent performances for photocatalytic applications. In most cases, anodization of titanium foil leads to the formation of a bamboo-type TiO_2 nanotube structure [30–34].

The simplest way of describing the optical properties of such crystals is the use of the Bruggemann effective medium approximation. According to the Bruggeman theory, the concentrations of matrix media and inclusions should be approximately the same [35]. Optically speaking, when light propagates along nanotubes, bamboo-type TiO_2 nanotubes are one-dimensional PCs due to refractive index modulation. The application of the effective medium theory may be quantitatively inaccurate. So, in this study, we demonstrate numerically the possibility of exciting TPs in the bamboo-type TiO_2 nanotube PCs without the effective medium approximation, but by solving a 3D problem using the finite-difference time-domain (FDTD) method. The effect of various structural parameters on the spectral properties and ehe integral absorption of the structure with different metallic layer coating is calculate, which can be important for photocatalytic applications.

2. Structure Design

Figure 1a shows a schematic of the investigated structure. The PC consists of a triangular lattice of TiO_2 cylinders with a length of L = 6 μm, an outer radius of r = 55 nm, wall thickness h and the refractive index equal 2.51. Along the cylinder surface, there are 40 TiO_2 ring thickenings with outer radius R. The parameters of the structure are given in Table 1.

Table 1. Calculation parameters.

Symbol	Structural Parameter	Value
L	TiO_2 nanotube length	6 μm
r	Outer radius	55 nm
h	Wall thickness	10 nm
R	Outer radius of ring thickenings	65 nm
d_1	Distance between rings	105 nm
d_2	Height of ring thickenings	45 nm
d_m	Metallic layer thickness	

The PC are conjugated with different metal thin films from gold [36], titanium [37] or titanium nitride [37] with thickness d_m. The investigated structure is placed in a medium with a refractive index n_{el} = 1.403, corresponding to propionitrile electrolyte.

The reflectance spectra of the structure was calculated by finite difference time domain (FDTD) method. The FDTD does not use approximations and is accurate for classical electrodynamics. The equations are solved by the finite difference method on two nested structured rectangular grids, one of which is intended for calculating electric fields, the other for magnetic ones. The method allows one to obtain the transmission, reflection, and absorption spectra of the system under study, as well as the field distribution within the computational domain in one calculation, taking into account both the geometric structure of the system under study and the optical properties of the materials used. The sketch view

of the simmulation box is shown in Figure 1b. The reflectance is calculated at the top of simulation box. The periodic boundary conditions (PBC) are set at the lateral boundaries of the simulation box, while on the top and bottom interfaces, the perfectly matched layer (PML) boundary conditions are used. The PC structure is illuminated from the top by a plane wave with the **E** vectors in the *z0y* plane.
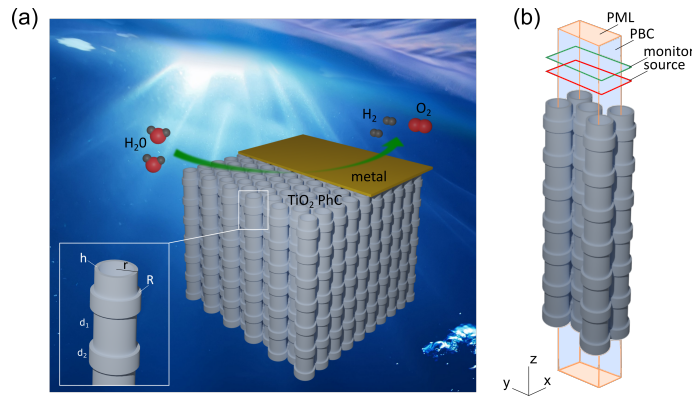

Figure 1. (**a**) Sketch view of the titanium oxide nanotubes arranged in hexagonal array for photocatalytic water splitting. Tamm plasmon polariton (TPP) transforms the light energy under the metal film for frequencies in stop-band of photonic crystal (PC). PC parameters are defined in the inset and specified in Table 1. (**b**) Finite difference time domain simulation box, the upper side is set to perfectly matched layer (PML), the vertical side is set to periodic boundary conditions (PBC), the monitor of reflected field is places above the radiation source.

3. Results and Discussion

Figure 2 presents the calculated reflectance spectra of a solitary PC with different wall thicknesses h. It can be clearly seen that the TiO$_2$ PC has a photonic band gap, the position of which is determined by the nanotube wall thickness. As the wall thickness increases, the band gap shifts to the long-wavelength spectral range. In particular, when wall thickness h changes from 5 to 25 nm, the band gap center shifts by 70 nm. This is caused by an increase in the effective permittivity of the PC optical layers with an increase in the nanotube wall thickness.
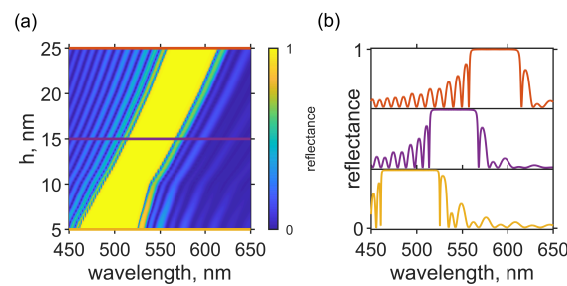

Figure 2. (**a**) Reflectance spectra of the TiO$_2$ photonic crystal. Increase of the TiO$_2$ nanotube wall thickness h redshifts the bandgap; (**b**) Cross sections of the reflectance map for h = 5 nm, h = 15 nm and h = 25 nm, respectively.

The deposition of a metallic layer onto the tubes leads to a qualitative change in the spectral properties of the structures and makes it possible to block light between the metallic layer and PC. In this case, the TPP forms. It should be noted that the spectral properties of such a localized state can be described within the temporal coupled-mode theory.

The spectral properties of the TPP can be predict by temporal coupled mode theory (TCMT) [38,39]. This theory describes the behavior of the field amplitude near the resonance. According to TCMT any state (resonance) has its own frequency ω_0 and number N of energy channels outside and inside the resonance. Then, the energy loss in the channels is

described by the relaxation times τ_l or relaxation rate $\gamma_l = 1/\tau_l$, where $l = 1, 2, \ldots, N$. If the energy leaves the resonance along two energy channels with relaxation times τ_1 and τ_2, then the relaxation time of the state is determined as $1/\tau = 1/\tau_1 + 1/\tau_2$. In the presented structure three energy channels contribute to the TPP formation. We denote the energy relaxation to the metal transmission, metal absorption and PC transmission channels as γ_m, γ_A and γ_{PC}, respectively. The rate of relaxation in each channel is proportional to the power flow in it divided by the energy accumulated in the TPP. So, the relaxation rates are related to corresponding energy coefficients of the structure as [40]:

$$\gamma_m : \gamma_A : \gamma_{PC} = T_m : A_m : T_{PC}. \tag{1}$$

In the PC band gap the quantity γ_{PC} can be ignored. Then, critical coupling condition (1) can be written in the form:

$$\gamma_m = \gamma_A; \quad \gamma_{PC} = 0 \Leftrightarrow T_m = A_m; \quad T_{PC} = 0. \tag{2}$$

This equation can be solved graphically. Let as consider the metal film with refractive index n_m, located between the first layer of PC with refractive index n_f and electrolyte with the refractive indices n_{el}. In this case, the transmittance, reflectance and absorptance of the metallic film are determined using the Airy formulas:

$$T_m = \left| \frac{t_{12} + t_{23} e^{i\beta}}{1 + r_{12} r_{23} e^{2i\beta}} \right|^2, \quad R_m = \left| \frac{r_{12} + r_{23} e^{2i\beta}}{1 + r_{12} r_{23} e^{2i\beta}} \right|^2, \tag{3}$$
$$A_m = 1 - T_m - R_m,$$

where $\beta = 2\pi n_m d_m / \lambda$ is the phase incoming during the passage of the wave through the layer; λ is the wavelength; d_m is the metallic film thickness $t_{12} = 2n_f/(n_f + n_m)$, $r_{12} = (n_f - n_m)/(n_f + n_m)$ and $t_{23} = 2n_m/(n_m + n_{el})$, $r_{23} = (n_m - n_{el})/(n_m + n_{el})$ – are the amplitudes of transmission and reflection at the interfaces 1–2 and 2–3.

Figures 3a–c show the differences between transmission and absorption of the gold, titanium and titanium nitride films of different thickness. According to the presented theory, critical coupling condition is met when the transmittance and absorptance of the metallic films are equal, or, in our case, when their difference is zero. It can be seen in Figure 3 that this equality is achieved by tuning the metallic film thickness.

The metallic film thickness dependences of the transmittance and absorptance at a constant wavelength of $\lambda = 515$ nm are presented in Figures 3d–f. It can be seen that the critical coupling condition for the films of three types is satisfied at d $_{Au}$ = 35.8 nm, d_{Ti} = 11.2 nm and d_{TiN} = 28 nm. As can be seen from Figure 3g in the scheme of TPP excitation through the Au layer, the critical coupling conditions are established at the lower transmittances and absorptances, i.e., at lower energy relaxation rates, the sum of which determines the resonance linewidth in the spectrum. In addition, it can be seen that when the PC is conjugated with the Ti or TiN film, the critical coupling conditions are established at the high transmittance and absorptance. As a result, the spectral linewidth corresponding to the TPP increases. Then, the broadband TPP is localized at the interface between the PC and metallic film. Thus, the coupled-mode theory can predict the energy coefficients at the TPP frequencies and spectral linewidth.

To demonstrate the possibility of the TPP excitation, the reflectance spectra of the PC conjugated with different metallic films were calculated. The results are shown in Figure 4.

It can be seen, that the minima of the reflectance in the PC band gap are achieved at certain metallic film thicknesses. These minima correspond to the critical coupling condition of the incident field with the TPP. Almost zero reflectance at the TPP wavelength suggests that the radiation incident onto the structure is totally absorbed by the metallic film (see Figure 5). The calculation showed that the critical coupling condition is met at thicknesses of 35.2, 12.5, and 22 nm for the gold, titanium, and titanium nitride films, respectively. It should be noted that, as predicted by the coupled-mode theory, the linewidths are

different. The narrowest line corresponds to the conjugation of the PC with the gold film, while for titanium and titanium nitride films linewidth is comparable with the PC band gap. In other words, in this case, a broadband Tamm plasmon polariton (TPP) is excited. Importantly, the results obtained by two different methods are in good agreement (see Table 2), although the coupled-mode theory is only applicable to the resonances with a Q factor above 30.
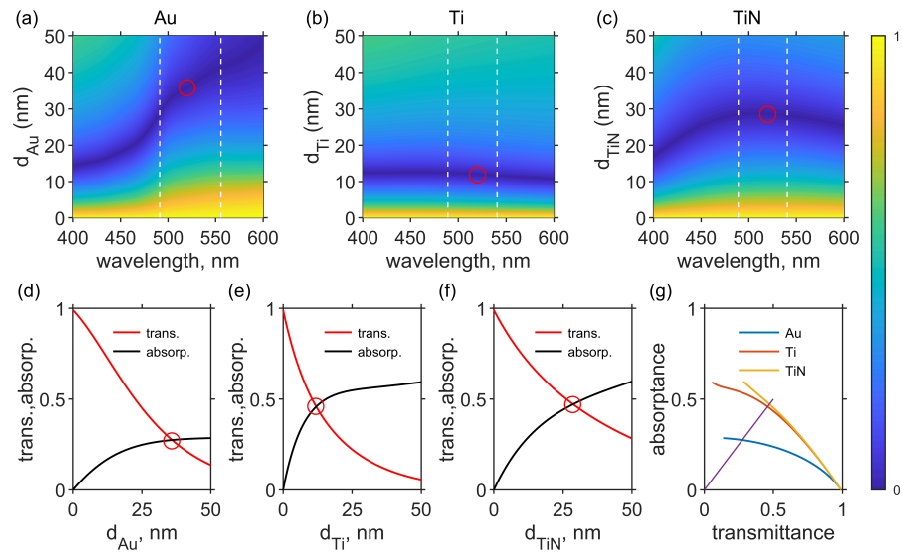

Figure 3. (**a**–**c**) $|T_m - A_m|$ of the different metal film calculated by Equation (3) in range from 400 to 600 nm. The white lines shows the edges of the photonic crystal band gap. (**d**–**f**) Dependence of the transmittance and absorptance of the metal film on its thickness. (**g**) Dependence of absorptance of the metallic film on its transmittance for different film materials. The $A_m(T_m)$ curves cross the critical coupling condition curve (purple line). The cross points represent the critical coupling conditions for TPP resonance for different materials of the metal layer. The wavelength is $\lambda = 515$ nm.
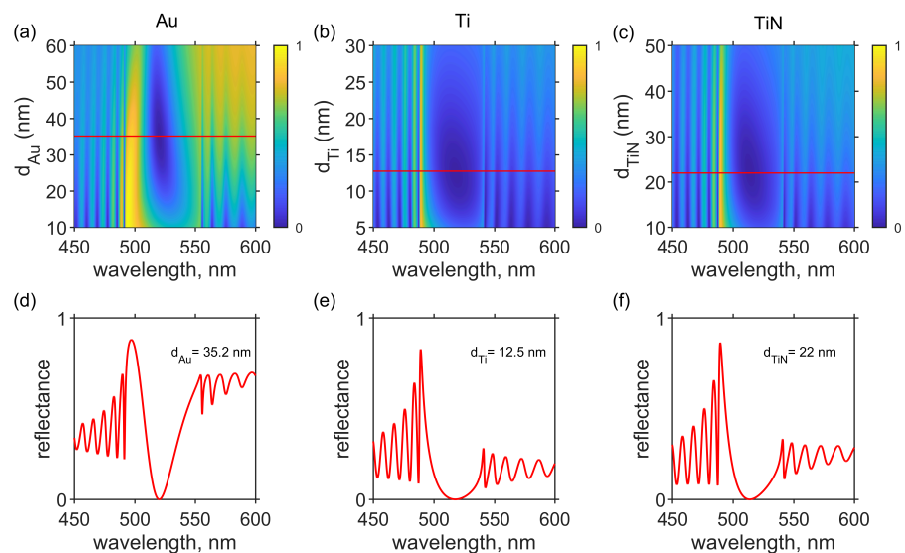

Figure 4. Reflectance spectra of the structures consisting of the PC conjugated with (**a**) the gold, (**b**) titanium, and (**c**) titanium nitride film of different thicknesses. (**d**–**f**) Reflectance spectra of the corresponding structures under the condition of critical coupling of the incident field with the TPP.

Table 2. Thicknesses of the metal films defined by TCMT and transfer matrix methods.

Metal	Thickness Defined by TCMT	Thickness Defined by Transfer Matrix
Au	35.8 nm	35.2 nm
Ti	11.2 nm	12.5 nm
TiN	28 nm	22 nm

For photocatalytic applications, the absorption characteristics are of crucial importance. Here, a key quantity is the integral absorption of a structure, i.e., the absorption in the metallic layer normalized to the solar radiation spectrum [22,23]

$$A_{total} = \frac{\int_{\lambda_1}^{\lambda_2} A(\lambda) S(\lambda) d\lambda}{\int_{\lambda_1}^{\lambda_2} S(\lambda) d\lambda}, \tag{4}$$

where λ_1 and λ_2 are the boundaries of the spectral range, $A(\lambda)$ is the absorption of a structure, and $S(\lambda)$ is the solar radiation spectra (air mass(AM) 1.5). The results of the calculation are presented in Figure 5. It can be seen that the highest total absorption in the investigated wavelength range is obtained in the structure with the PC conjugated with the titanium film. In this case, we have $A_{total} = 58.2\%$, while the values for the gold and titanium nitride films are 42.5 and 55.7%, respectively.
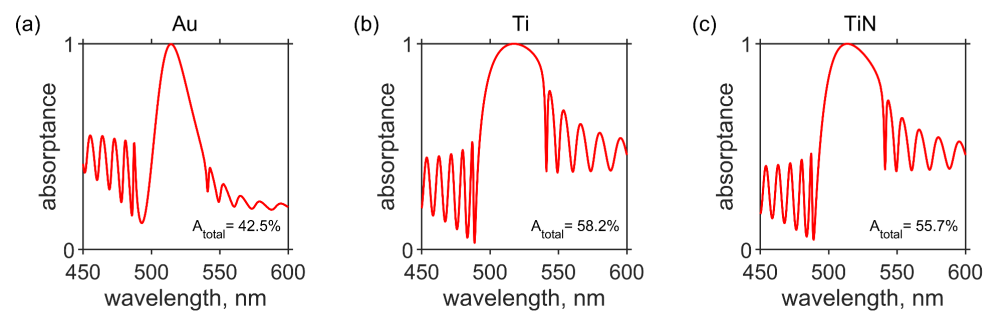

Figure 5. Absorptance spectra of the investigated structure consisting of the PC conjugated with (**a**) the gold, (**b**) titanium, and (**c**) titanium nitride film. The corresponding total absorptances are shown in the lower right-hand corner. Metal thicknesses are the same as in Figure 4.

4. Conclusions

Using 3D modeling, the occurrence of Tamm plasmons in the anodic TiO$_2$ nanotube photonic crystals was predicted. The effect of the nanotube thickness on the spectral position of the photonic bandgap was examined. The gold, titanium, and titanium nitride metallic layers coating the PC were investigated. Using the temporal coupled-mode theory, the optimum thicknesses of the metallic layers were determined. The theoretical results turned out to be consistent with the data of the direct calculation. In each case, the absorption band appeared in the reflectance and absorptance spectra of the structure. The calculation of the integral absorption of the structure in the range of 450–600 nm yielded the highest value (up to 58.2%) for the structure with the titanium nitride coating, which can be important for photocatalytic applications such as a water splitting.

Author Contributions: Conceptualization, I.V.T., S.Y.V. and V.F.S.; methodology and software, M.V.P. and R.G.B.; validation, M.V.P., R.G.B. and I.I.R.; writing—original draft preparation, M.V.P.; visualization, R.G.B. and I.I.R.; supervision, V.F.S. and S.Y.V. All authors have read and agreed to the published version of the manuscript.

Institutional Review Board Statement: Not applicable.

Informed Consent Statement: Not applicable.

Data Availability Statement: The data presented in this study are available upon reasonable request from the corresponding author.

Conflicts of Interest: The authors declare no conflict of interest.

References

1. Kavokin, A.V.; Shelykh, I.A.; Malpuech, G. Lossless interface modes at the boundary between two periodic dielectric structures. *Phys. Rev. B* **2005**, *72*, 233102. [CrossRef]
2. Vinogradov, A.P.; Dorofeenko, A.V.; Erokhin, S.G.; Inoue, M.; Lisyansky, A.A.; Merzlikin, A.M.; Granovsky, A.B. Surface state peculiarities in one-dimensional photonic crystal interfaces. *Phys. Rev. B* **2006**, *74*, 045128. [CrossRef]
3. Kaliteevski, M.; Iorsh, I.; Brand, S.; Abram, R.A.; Chamberlain, J.M.; Kavokin, A.V.; Shelykh, I.A. Tamm plasmon-polaritons: Possible electromagnetic states at the interface of a metal and a dielectric Bragg mirror. *Phys. Rev. B* **2007**, *76*, 165415. [CrossRef]
4. Sasin, M.; Seisyan, R.; Kalitteevski, M.; Brand, S.; Abram, R.; Chamberlain, J.; Egorov, A.Y.; Vasil'Ev, A.; Mikhrin, V.; Kavokin, A. Tamm plasmon polaritons: Slow and spatially compact light. *Appl. Phys. Lett.* **2008**, *92*, 251112. [CrossRef]
5. Goto, T.; Dorofeenko, A.V.; Merzlikin, A.M.; Baryshev, A.V.; Vinogradov, A.P.; Inoue, M.; Lisyansky, A.A.; Granovsky, A.B. Optical Tamm States in One-Dimensional Magnetophotonic Structures. *Phys. Rev. Lett.* **2008**, *101*, 113902. [CrossRef]
6. Chen, H.; Chen, Z.; Yang, H.; Wen, L.; Yi, Z.; Zhou, Z.; Dai, B.; Zhang, J.; Wu, X.; Wu, P. Multi-mode surface plasmon resonance absorber based on dart-type single-layer graphene. *RSC Adv.* **2022**, *12*, 7821–7829. [CrossRef]
7. Deng, Y.; Cao, G.; Wu, Y.; Zhou, X.; Liao, W. Theoretical description of dynamic transmission characteristics in MDM waveguide aperture-side-coupled with ring cavity. *Plasmonics* **2015**, *10*, 1537–1543. [CrossRef]
8. Pankin, P.S.; Sutormin, V.S.; Gunyakov, V.A.; Zelenov, F.V.; Tambasov, I.A.; Masyugin, A.N.; Volochaev, M.N.; Baron, F.A.; Chen, K.P.; Zyryanov, V.Y.; et al. Experimental implementation of tunable hybrid Tamm-microcavity modes. *Appl. Phys. Lett.* **2021**, *119*, 161107. [CrossRef]
9. Huang, S.G.; Chen, K.P.; Jeng, S.C. Phase sensitive sensor on Tamm plasmon devices. *Opt. Mater. Express* **2017**, *7*, 1267–1273. [CrossRef]
10. Buchnev, O.; Belosludtsev, A.; Reshetnyak, V.; Evans, D.R.; Fedotov, V.A. Observing and controlling a Tamm plasmon at the interface with a metasurface. *Nanophotonics* **2020**, *9*, 897–903. [CrossRef]
11. Chen, J.; Zhang, Q.; Peng, C.; Tang, C.; Shen, X.; Deng, L.; Park, G.S. Optical Cavity-Enhanced Localized Surface Plasmon Resonance for High-Quality Sensing. *IEEE Photonics Technol. Lett.* **2018**, *30*, 728–731. [CrossRef]
12. Thompson, R.J.; Siday, T.; Glass, S.; Luk, T.S.; Reno, J.L.; Brener, I.; Mitrofanov, O. Optically thin hybrid cavity for terahertz photo-conductive detectors. *Appl. Phys. Lett.* **2017**, *110*, 041105. [CrossRef]
13. Zhang, W.L.; Wang, F.; Rao, Y.J.; Jiang, Y. Novel sensing concept based on optical Tamm plasmon. *Opt. Express* **2014**, *22*, 14524–14529. [CrossRef]
14. Jeng, S.C. Applications of Tamm plasmon-liquid crystal devices. *Liq. Cryst.* **2020**, *47*, 1223–1231. . 2020.1733114. [CrossRef]
15. Wang, L.; Cai, W.; Bie, M.; Zhang, X.; Xu, J. Zak phase and topological plasmonic Tamm states in one-dimensional plasmonic crystals. *Opt. Express* **2018**, *26*, 28963–28975. [CrossRef] [PubMed]
16. Lakhtakia, A.; McCall, M. Sculptured thin films as ultranarrow-bandpass circular-polarization filters. *Opt. Commun.* **1999**, *168*, 457–465. . [CrossRef]
17. Zhou, W.; Dridi, M.; Suh, J.Y.; Kim, C.H.; Co, D.T.; Wasielewski, M.R.; Schatz, G.C.; Odom, T.W. Lasing action in strongly coupled plasmonic nanocavity arrays. *Nat. Nanotechnol.* **2013**, *8*, 506–511. [CrossRef]
18. Symonds, C.; Lheureux, G.; Hugonin, J.P.; Greffet, J.J.; Laverdant, J.; Brucoli, G.; Lemaitre, A.; Senellart, P.; Bellessa, J. Confined Tamm Plasmon Lasers. *Nano Lett.* **2013**, *13*, 3179–3184. [CrossRef]
19. Fang, M.; Shi, F.; Chen, Y. Unidirectional all-optical absorption switch based on optical Tamm state in nonlinear plasmonic waveguide. *Plasmonics* **2016**, *11*, 197–203. [CrossRef]
20. Bikbaev, R.G.; Vetrov, S.Y.; Timofeev, I.V. Epsilon-Near-Zero Absorber by Tamm Plasmon Polariton. *Photonics* **2019**, *6*, 28. [CrossRef]
21. Pühringer, G.; Consani, C.; Jannesari, R.; Fleury, C.; Dubois, F.; Spettel, J.; Dao, T.D.; Stocker, G.; Grille, T.; Jakoby, B. Design of a Slab Tamm Plasmon Resonator Coupled to a Multistrip Array Waveguide for the Mid Infrared. *Sensors* **2022**, *22*, 2968. [CrossRef] [PubMed]
22. Zhang, X.L.; Song, J.F.; Li, X.B.; Feng, J.; Sun, H.B. Optical Tamm states enhanced broad-band absorption of organic solar cells. *Appl. Phys. Lett.* **2012**, *101*, 243901. [CrossRef]
23. Bikbaev, R.G.; Vetrov, S.Y.; Timofeev, I.V.; Shabanov, V.F. Photosensitivity and reflectivity of the active layer in a Tamm-plasmon-polariton-based organic solar cell. *Appl. Opt.* **2021**, *60*, 3338–3343. [CrossRef] [PubMed]
24. Vyunishev, A.M.; Bikbaev, R.G.; Svyakhovskiy, S.E.; Timofeev, I.V.; Pankin, P.S.; Evlashin, S.A.; Vetrov, S.Y.; Myslivets, S.A.; Arkhipkin, V.G. Broadband Tamm plasmon polariton. *J. Opt. Soc. Am. B* **2019**, *36*, 2299–2305. [CrossRef]

25. Pyatnov, M.V.; Bikbaev, R.G.; Timofeev, I.V.; Ryzhkov, I.I.; Vetrov, S.Y.; Shabanov, V.F. Broadband Tamm Plasmons in Chirped Photonic Crystals for Light-Induced Water Splitting. *Nanomaterials* **2022**, *12*, 928. [CrossRef]

26. Eliseev, A.A.; Lukashin, A.V. *Funtional'nye Nanomaterialy (Functional Nanomaterials)*; Fizmatlit: Moscow, Russia, 2010; p. 456.

27. Bobrovsky, A.Y.; Svyakhovskiy, S.; Roslyakov, I.V.; Piryazev, A.A.; Ivanov, D.A.; Shibaev, V.P.; Cigl, M.; Hamplová, V.; Bubnov, A. Photoinduced Split of the Cavity Mode in Photonic Crystals Based on Porous Silicon Filled with Photochromic Azobenzene-Containing Substances. *ACS Appl. Pol. Mat.* **2022**, *4*, 7387–7396. [CrossRef]

28. Law, C.S.; Lim, S.Y.; Abell, A.D.; Voelcker, N.H.; Santos, A. Nanoporous anodic alumina photonic crystals for optical chemo-and biosensing: Fundamentals, advances, and perspectives. *Nanomaterials* **2018**, *8*, 788. [CrossRef]

29. Roy, P.; Berger, S.; Schmuki, P. TiO_2 Nanotubes: Synthesis and Applications. *Angew. Chem. Int. Ed.* **2011**, *50*, 2904–2939.

30. Ermolaev, G.A.; Kushnir, S.E.; Sapoletova, N.A.; Napolskii, K.S. Titania photonic crystals with precise photonic band gap position via anodizing with voltage versus optical path length modulation. *Nanomaterials* **2019**, *9*, 651. [CrossRef]

31. Sadykov, A.; Kushnir, S.; Sapoletova, N.; Ivanov, V.; Napolskii, K. Anodic titania photonic crystals with high reflectance within photonic band gap via pore shape engineering. *Scr. Mater.* **2020**, *178*, 13–17. . 2019.10.044. [CrossRef]

32. Li, J.F.; Wang, J.; Wang, X.T.; Wang, X.G.; Li, Y.; Wang, C.W. Bandgap engineering of TiO_2 nanotube photonic crystals for enhancement of photocatalytic capability. *CrystEngComm* **2020**, *22*, 1929–1938. [CrossRef]

33. Guo, M.; Xie, K.; Wang, Y.; Zhou, L.; Huang, H. Aperiodic TiO_2 nanotube photonic crystal: Full-visible-spectrum solar light harvesting in photovoltaic devices. *Sci. Rep.* **2014**, *4*, 6442. [CrossRef] [PubMed]

34. Guo, M.; Su, H.; Zhang, J.; Liu, L.; Fu, N.; Yong, Z.; Huang, H.; Xie, K. Broadband and omnidirectional light harvesting enhancement in photovoltaic devices with aperiodic TiO_2 nanotube photonic crystal. *J. Power Sources* **2017**, *345*, 12–20. . [CrossRef]

35. Golovan, L.A.; Timoshenko, V.Y.; Kashkarov, P.K. Optical properties of porous-system-based nanocomposites. *Physics-Uspekhi* **2007**, *50*, 595. [CrossRef]

36. Johnson, P.B.; Christy, R.W. Optical Constants of the Noble Metals. *Phys. Rev. B* **1972**, *6*, 4370–4379. . physrevb.6.4370. [CrossRef]

37. Palik, E.D. *Handbook of Optical Constants of Solids*; Academic Press: Boca Raton, FL, USA, 2014.

38. Haus, H. *Waves and Fields in Optoelectronics*; Prentice-Hall, Inc.: Englewood Cliffs, NJ, USA, 1984; p. 402.

39. John, S.; Joannopoulos, D.; Winn, J.N.; Meade, R.D. *Photonic Crystals: Molding the Flow of Light*; Princeton University of Press: Princeton, NJ, USA, 2008.

40. Yang, Z.Y.; Ishii, S.; Yokoyama, T.; Dao, T.D.; Sun, M.G.; Pankin, P.S.; Timofeev, I.V.; Nagao, T.; Chen, K.P. Narrowband Wavelength Selective Thermal Emitters by Confined Tamm Plasmon Polaritons. *ACS Photonics* **2017**, *4*, 2212–2219. [CrossRef]